Available online at BCREC website: https://bcrec.id

Bulletin of Chemical Reaction Engineering & Catalysis, 18 (1) 2023, 118-130

Research Article

Synthesis of Bimetallic Metal-Organic Frameworks (MOFs) La-Y-PTC for Enhanced Dyes Photocatalytic Degradation

Adawiah Adawiah[1,*], Muhammad Shofyan Gunawan[2], Isalmi Aziz[2], Wulandari Oktavia[2]

[1]Integrated Laboratory Centre, Faculty of Science and Technology UIN Syarif Hidayatullah Jakarta, Jl. Ir. H. Juanda No. 95 Ciputat South Tangerang 15412, Indonesia.
[2]Department of Chemistry, Faculty of Science and Technology UIN Syarif Hidayatullah Jakarta, Jl. Ir. H. Juanda No. 95 Ciputat Tangerang Selatan 15412, Indonesia.

Received: 11th October 2022; Revised: 18th March 2023; Accepted: 20th March 2023
Available online: 27th March 2023; Published regularly: April 2023

Abstract

Metal-Organic Frameworks (MOFs) is widely utilized as photocatalysts in dye photocatalytic degradation. This study successfully synthesized bimetallic MOFs La-Y-PTC by the solvothermal method. The synthesized La-Y-PTC has a diffractogram pattern with a value of 2θ = 5.69°; 9.57°; 16.8°; 20.05°; 24.8°; 26.15°; 29.77° and 41.93° with a crystal size of 21.45 nm. The La-Y-PTC has symmetric and asymmetric (COO−) at 1591 and 1433 cm^{-1}, La−O and Y−O groups at 596 and 659 cm^{-1} and a band gap energy of 2.16 eV. Scanning Electron Microscope analysis showed that the morphology of La-Y-PTC is spherical with a particle size of 354.307 nm. La-Y-PTC degrades methylene blue and methyl orange at pH 2 with a degradation efficiency of 69.57% and 93.63%, respectively, under 250 watts of mercury lamp irradiation for 180 min with hydroxyl radical species as a dominant species that play a role in methylene blue and methyl orange degradations.

Keywords: Degradation; photocatalyst; methylene blue; methyl orange; La-Y-PTC

How to Cite: A. Adawiah, M.S. Gunawan, I. Aziz, W. Oktavia (2023). Synthesis of Bimetallic Metal-Organic Frameworks (MOFs) La-Y-PTC for Enhanced Dyes Photocatalytic Degradation. *Bulletin of Chemical Reaction Engineering & Catalysis*, 18(1), 118-130 (doi: 10.9767/bcrec.16130)

Permalink/DOI: https://doi.org/10.9767/bcrec.16130

1. Introduction

The industry plays an essential role in the aquatic ecosystems' pollution due to the wastewater produced. Priya *et al.* explained that around 90% of waste in developing countries is disposed of in water systems without prior treatment [1]. The textile and dye industry generates as much as 20% of industrial wastewater [2], which contains many organic pollutants like methylene blue and methyl orange [3]. Both methylene blue and methyl orange are highly toxic, carcinogenic [4], and challenging to degrade, contributing to environmental and human health problems [5].

Several methods have been applied in dye contaminant elimination, like adsorption, coagulation, and photocatalytic degradation. Adsorption is binding a fluid, liquid, or gas by a particle due to attractive forces between molecules [6,7]. Coagulation is the conglomeration of small particles into larger particles to form a precipitate by providing a coagulant substance. In comparison, photocatalytic degradation is a chemical reaction involving a semiconductor catalyst with a photon as an energy source. Of the three techniques, photocatalytic degradation is con-

* Corresponding Author.
Email: adawiah@uinjkt.ac.id (A. Adawiah);
Telp: +62-21-7493606, Fax: +62-21-7493315

sidered the most efficient technique, because it produces a final product that is more environmentally friendly, like CO_2 and H_2O [8-9].

The metal-organic framework (MOF) is a semiconductor material widely employed in dye photodegradation due to its unique properties, including a large surface area, uniform distribution of active sites, and tunable band gap energy [10]. Zulys *et al.* synthesized La-PTC MOFs, which degraded only methyl orange 10 ppm by 64.74% for 240 min under visible light irradiation [11]. Adawiah *et al.* succeeded in synthesizing Y-PTC, which can degrade methylene blue 10 ppm and methyl orange 10 ppm by 62.57% and 50.89%, respectively, for 240 min on mercury lamp irradiation [12].

On the other hand, Arora *et al.* reported that Fe-BDC MOFs generated a degradation efficiency of 94.74% methylene blue 5 ppm within 24 h [13]. Herrera *et al.* successfully synthesized Zn-BDC MOFs with a 10 ppm methylene blue degradation efficiency of 62.3% in 3 h under the Xe lamp irradiation [14]. Tiwari *et al.* reported that combining iron(III) and zinc(II) metal ion to construct Fe-Zn-BDC bimetallic MOFs provide an increase in methylene blue (10 ppm) degradation with degradation efficiency of 57% in 90 min under visible light irradiation [15]. These studies showed that Fe-Zn-BDC bimetallic MOFs' degradation activity is higher than their monometallic forms.

Therefore, this study aims to fabricate La-Y-PTC bimetallic MOF by combining lanthanum and yttrium metal ions and perylene-3,4,9,10-tetracarboxylic (PTC) as an organic linker to increase the photocatalytic activity of La-PTC and Y-PTC monometallic MOFs. The obtained MOF is expected can degrade not only for methylene blue but also for methyl orange.

2. Materials and Methods

2.1 Materials

The materials in this study were used without any purification. These are lanthanum nitrate hexahydrate ($La(NO_3)_3.6H_2O$) (EMSURE, Merck), perylene-3,4,9,10-tetracarboxylic dianhydride (PTCDA) (97%, Sigma-Aldrich), sodium hydroxide (NaOH) (EMSURE, Merck), yttrium nitrate hexahydrate ($Y(NO_3)_3.6H_2O$) (EMSURE, Merck), ethanol (EtOH) 96% (technical grade), methanol (MeOH) (EMSURE, Merck), hydrogen peroxide (H_2O_2) (EMSURE, Merck), tertier butanol (tert-BuOH) (EMSURE, Merck), barium sulfate ($BaSO_4$) (EMSURE, Merck), potassium bromide (KBr) (EMSURE, Merck), N,N-dimethyl formamide (DMF) (99.8%, Loba Chemie PVT, LTD) methylene blue (MB) (EMSURE, Merck), distilled water (H_2O), and methyl orange (MO) (EMSURE, Merck).

2.2 Preparation of Natrium Perylene-3,4,9,10-tetracarboxylic (Na_4PTC) from Perylene-3,4,9,10-tetracarboxylic dianhydride (PTCDA)

PTCDA (0.5 g) was dissolved in 50 mL of distilled water. Then, NaOH (0.356 g) was added while stirring with a magnetic stirrer at 300 rpm for 60 min. Next, the solution was filtered, and the filtrate was added to excess ethanol to obtain a yellow precipitate. The resulting yellow precipitate of Na_4PTC was filtered, washed with ethanol to a neutral pH and dried at room temperature for 24 h.

2.3 Synthesis MOFs Bimetallic La-Y-PTC

The synthesis of La-Y-PTC bimetallic MOFs was carried out by the solvothermal method. The preparation began with dissolving the $La(NO_3)_3.6H_2O$, $Y(NO_3)_3.6H_2O$ and Na_4PTC with a molar ratio of La:Y:Na_4PTC (1:2:1 mmol) into DMF 5 mL and H_2O 25 mL. Then, the mixture was magnetically stirred for 60 min at 300 rpm and transferred to a stainless Teflon-line autoclave. Next, it was heated at 170 °C for 24 h. The mixture was cooled for 24 h at room temperature. Finally, the brown precipitate was filtered and washed with distilled water to a neutral pH and then dried at 70 °C overnight.

2.4 Characterization of MOFs La-Y-PTC

The synthesized La-Y-PTC was characterized with Fourier Transform Infra-Red (FTIR) Prestige 21 Shimazu for functional group analysis, X-Ray Powder Diffraction (XRD) 7000 Maxima-X for diffraction pattern analysis and crystal size, UV-Vis Diffuse Reflectance Spectroscopy Agilent Carry 60 for band gap energy analysis and Scanning Electron Microscope-Energy Dispersive X-Ray (SEM) FEI Quanta 650 for morphological analysis and the elements contained therein.

2.5 Photocatalytic Activity Test of Bimetallic MOFs La-Y-PTC

The photocatalytic activity of bimetallic MOFs La-Y-PTC was analyzed using two dyes: methylene blue and methyl orange. First, the test was performed by dispersing La-Y-PTC into 50 mL of dye solution. Then the mixture was stirred at 300 rpm for 180 min in dark conditions and 250-watt mercury lamp illumination. Next, the suspension was taken every 30 min

with 2 mL. Finally, the suspension was centrifuged at 6000 rpm for 10 min, and dye absorbance was measured by UV-Vis spectrophotometer at 665 nm for methylene blue and 465 for methyl orange. The degradation efficiency of dyes was calculated using Equation (1):

$$Degradation\ Efficiency\ (\%) = \frac{A_0 - A_t}{A_0} \quad (1)$$

where, A_0 is initial dye absorbance, and A_t is dyes absorbance at t.

2.6 Determination of Dominant Species in Photocatalytic Degradation of Methylene blue and Methyl Orange

The dominant species in photocatalytic degradation of methylene blue and methyl orange was determined by adding sacrificial agents like H_2O_2, CH_3OH and tert-BuOH with a concentration of 0.1 M. Then, the suspension was magnetically stirred at 300 rpm for 180 min. Then, the suspension was taken every 30 min for as much as 2 mL and centrifuged at 6000 rpm for 10 min. The dye absorbance was measured by UV-Vis spectrophotometer at 665 nm for methylene blue and 465 for methyl orange. The degradation efficiency of dyes was calculated using Equation (1).

2.7 Methylene Blue and Methyl Orange Selectivity Test

The selectivity test of methylene blue and methyl orange was carried out under the same dye concentration, La-Y-PTC dosage, and initial pH of the solution. Selectivity analysis between methylene blue and methyl orange was performed by dividing the volume of the two dyes into 25 mL each. After that, the suspension was taken every 30 min for as much as 2 mL and centrifuged at 6000 rpm for 10 min. The dye concentration was measured by UV-Vis spectrophotometer at 665 nm for methylene blue and 465 for methyl orange. The degradation efficiency of dyes was calculated using Equation (1).

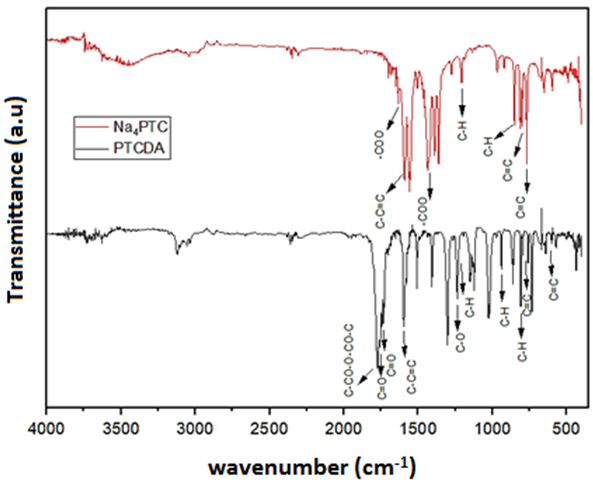

Figure 1. IR Spectrum of PTCDA and Na_4PTC.

2.8 The pHpcz of MOF La-Y-PTC Determination

The pHpzc of MOF La-Y-PTC was determined by the solid addition method [16]. 50 mg of La-Y-PTC was added to 100 mL conical flask containing of 40 mL NaCl 0.1 M at different initial pH (1-10), called pHi. Then, the pH was adjusted using NaOH 0.1 M and HCl 0.1 M. The final pH (pHf) was recorded after the electrolyte solution with La-Y-PTC was equilibrated for 24 h. Both negative and positive ΔpH were plotted against pHi. The pH which ΔpH becomes 0 is called pHpzc.

3. Results and Discussion

The conversion of PTCDA to Na_4PTC was confirmed by analysis of functional groups using Fourier Transform Infra-Red (FTIR) by looking at the shift in wavenumbers and the emergence of new spectra resulting from structural changes. The PTCDA and Na_4PTC FTIR spectra can be seen in Figure 1. The band at 1772 cm^{-1} confirmed the stretching vibration of the 5-ring cyclic anhydride group of PTCDA. Then, the peaks appeared at 1753 cm^{-1} and 1730 cm^{-1}, which was attributed to asymmetric and symmetric vibrations of cyclic anhydride (C=O) of PTCDA. Sharp peaks at 1234 cm^{-1} and 938 cm^{-1} were asymmetric and symmetric cluster (C–O) vibrations of the cyclic C–CO–O–CO–C of PTCDA. As shown in Figure 1, the characteristics of the anhydride in PTCDA no longer appear on the $Na_{1qaq}PTC$ FTIR spectrum.

The FTIR spectrum of Na_4PTC shows the peaks at 1633 and 1423 cm^{-1}, indicating (COO–) asymmetric and symmetric vibrations of carboxylic ions. It indicates that there is no longer a cyclic anhydride ring PTCDA but rather forms carboxylate ions. Then, the FTIR spectrum of Na_4PTC also does not show any absorption of the –OH group at 2500-3300 cm^{-1}, which explains that no –COOH formed because it has been wholly hydrolyzed by NaOH forming COO–Na group in Na_4PTC.

3.1 Characteristics of Bimetallic MOFs La-Y-PTC

Figure 2 shows the FTIR spectrum of La-Y-PTC. The peak at 3423 cm^{-1} is confirmed as an

O–H vibration derived from H_2O trapped in La-Y-PTC. Then, a peak at 1766 cm^{-1} indicates symmetric vibration (C=O) in La-Y-PTC. Asymmetric and symmetric peaks (–COO) in La-Y-PTC appear at 1591 and 1433 cm^{-1}. The vibration of C–H bends in the plane of aromatic rings is found in La-Y-PTC at 1212 cm^{-1}. It is found in La-Y-PTC, the La–O and Y–O groups at 596 and 659 cm^{-1}. Zulys *et al.* observed the peak at 576 cm^{-1}, which confirmed the La–O group in La-PTC [11]. Prabhu *et al.* obtained the La–O group at 512 cm^{-1} [17], Meanwhile, Adawiah *et al.* reported the presence Y–O group at 665 cm^{-1} [12]. In adition, Yang *et al.* obtained the Y–O group at 445 cm^{-1} [18]. Shadmehr *et al.* stated that the stretching vibration of metal-oxygen appeared at 400-800 cm^{-1} [19]. There are several shifts and the emergence of new peaks in La-Y-PTC compared to La-PTC and Y-PTC due to differences in the structure of MOFs so that they can be used as an indicator of the success of La-Y-PTC synthesis. Table 1 shows the wavenumber of the La-Y-PTC, La-PTC, and Y-PTC IR spectra.

Figure 3 shows the pattern of the La-Y-PTC diffractogram in which there are several diffraction peaks, including at 2θ = 5.69°, 9.57°, 16.8°; 20.05°; 24.8°, 26.15°; 29.77° and 41.93°. Meanwhile, the diffraction pattern with the highest intensity produced by La-PTC is at 2θ = 6.31°, 16.6°, 28.7°, 33.3° and 44.6° [11], while the diffraction pattern of Y-PTC is at 2θ= 17.04°, 26.27°, and 27.41° [12]. The difference in the absorption peak value indicates the difference in the crystal structure of the MOFs La-Y-PTC. It indicates that the La-Y-PTC was successfully formed. The calculation using the Debye Scherrer equation with the FWHM value at 2θ = 29.77° of 0.37876 obtained the crystal size of La-Y-PTC is 21.45 nm. In addition, the obtained XRD spectrum of La-Y-PTC did not show the peak for lanthanum or yttrium oxide compound like lanthanum oxide (La_2O_3), yttrium oxide (Y_2O_3), and lanthanum yttrium oxide (LaYO) (see the comparing spectrum in supplementary file).

The band gap energy can be obtained using the UV-Vis Diffuse Reflectance Spectrometry (DRS) instrument. The band gap energy is the energy between the valence band and the conduction band. It is the minimum energy limit

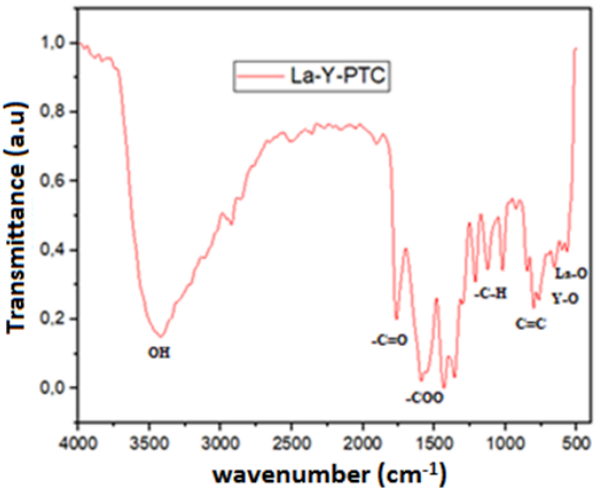

Figure 2. Infrared spectrum MOF La-Y-PTC.

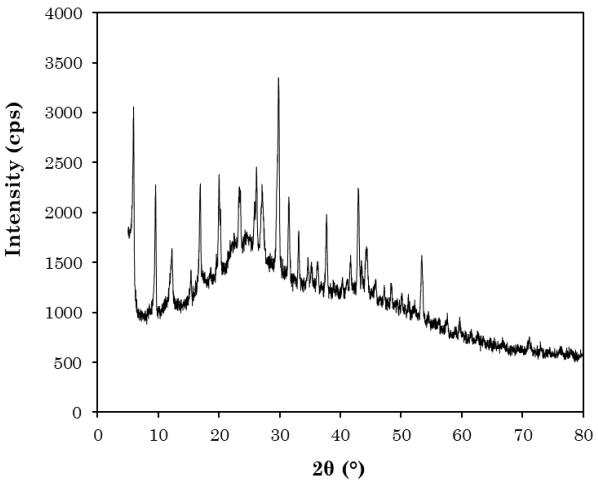

Figure 3. XRD spectrum of MOF La-Y-PTC.

Table 1. Infrared uptake peaks as well as La-PTC, Y-PTC and La-Y-PTC functional groups.

Wavenumbers (cm^{-1})			Information
La-PTC [14]	Y-PTC [15]	La-Y-PTC (this work)	
-	-	3423	Stretching OH (H_2O)
-	1772	1766	Symmetric vibration (C=O)
1530	1541	1591	Asymmetric vibration (–COO)
1434	1440	1433	Symmetric vibration (–COO)
1210	1212	1212	Bending (C–H) *in plane* aromatic ring
849, 808	846, 809	848, 803	Bending C–H *out of plane* aromatic ring
763	763	767	*Out of plane* C=C aromatic ring
-	655	659	stretching Y–O
572	-	596	stretching La–O

required by photocatalyst materials for photocatalytic processes [12]. Figure 4 exhibits that the band gap energy of bimetallic MOF La-Y-PTC is 2.16 eV or has an absorption region up to the visible light region of 574 nm. Previous research reported that monometallic MOF La-PTC and Y-PTC have band gap energy of 2.21 eV and 2.20 eV, respectively [11,12].

The arrangement of the Secondary Building Unit (SBU) of its metal ions modified the MOF's band gap energy. The structure of MOFs is composed of linker-SBU interface interactions, so linker-SBU interface interactions influence the electronic nature of MOFs. An increase in the size of the SBU unit can lead to a narrowing of the band gap energy (E_g) of MOFs. The difference in the size of the SBU from the metal used causes a shift in the band gap energy in the MOFs [20]. Chen *et al*. reported that two metals with the same ion radius and coordination bond are more likely to exist at the same level of SBU [21]. Lanthanum and yttrium have atomic radii that do not dif-

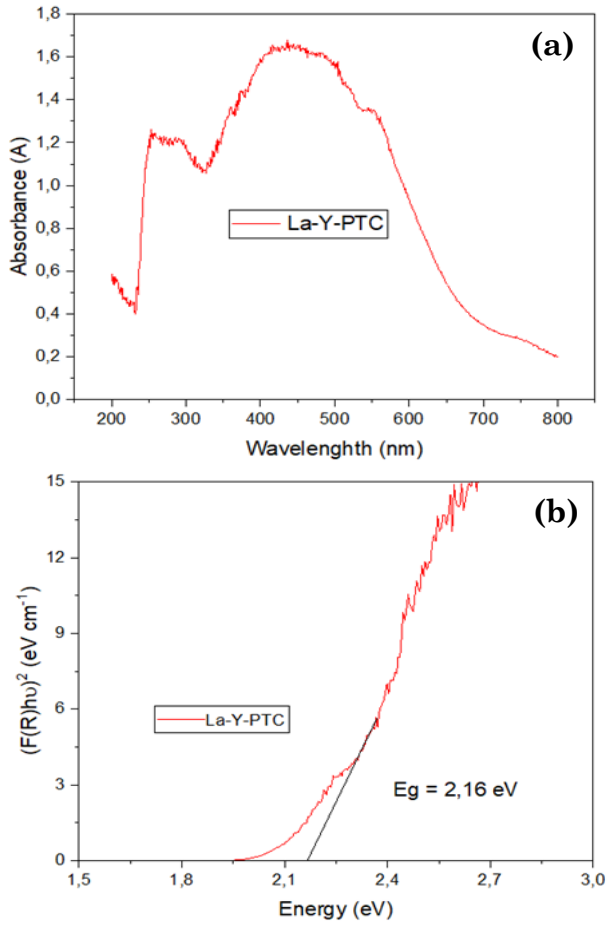

Figure 4. Band gap energy and absorbance spectrum MOFs La-Y-PTC (a) band gap energy bimetallic MOF La-Y-PTC (b).

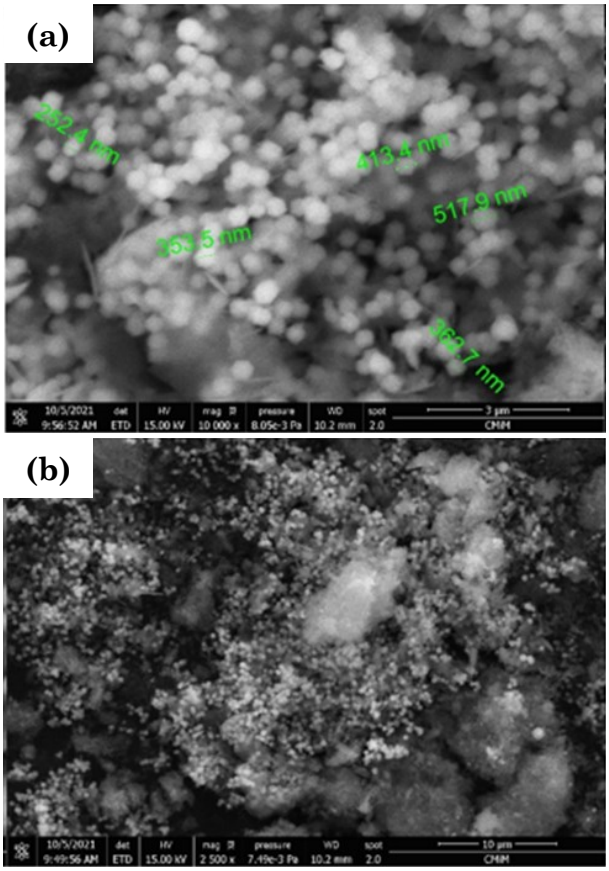

Figure 5. Morphology of MOFs La-Y-PTC (a) magnification 10000x, (b) magnification 2500x.

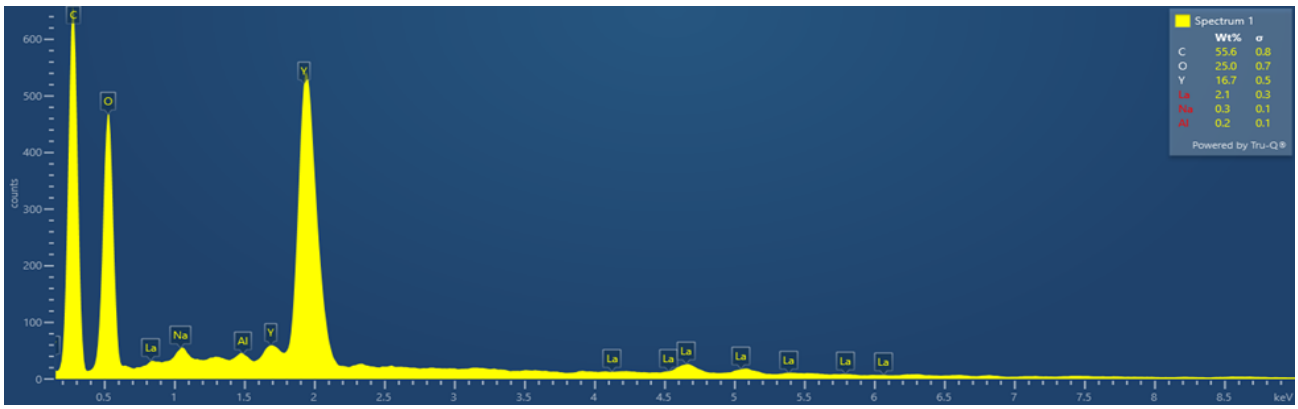

Figure 6. Spectrum EDS composition of elements MOFs La-Y-PTC.

fer much, namely 1.16 Å and 1.01 Å and are in one group [22].

Figure 5 shows the morphology of the MOFs La-Y-PTC shaped like spheres of varying diameters. As seen in Figure 5(a), the variation in MOFs diameter is 252.4 nm, 353.5 nm; 362.7 nm; 413.4 nm and 517.9 nm. However, there are still some impurities that look like cotton. Quantitative measurement by Image-J software resulted in the average particle size of bimetallic MOFs La-Y-PTC being 354.307 nm.

Figure 6 shows the EDS spectrum showing bimetallic MOFs La-Y-PTC consist carbon of 55.6%, oxygen of 25.0%, yttrium of 16.7%, lanthanum of 2.1%, sodium of 0.3% and aluminum of 0.2%. There are impurity elements, namely aluminum and sodium. However, the impurity elements have a small quantity. They are not coordinated with the COO− group of the Na_4PTC, which is confirmed by the absence of absorption bands for the Na−O and Al−O groups on the La-Y-PTC FTIR spectrum (Figure 2).

3.2 Methylene Blue Degradation by Bimetallic MOFs La-Y-PTC

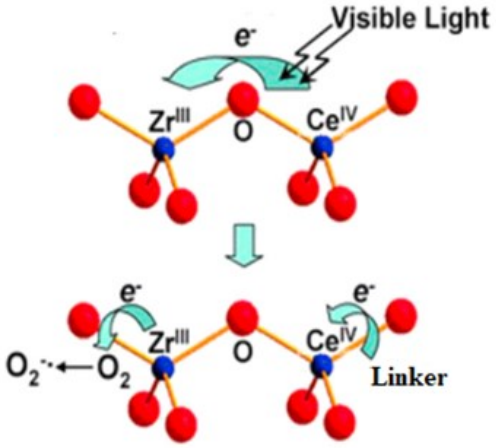

Figure 7. Illustration of metal-metal electron transfer and metal-linker Zr−O−Ce [24].

La-Y-PTC exhibits degradation efficiency of methylene blue of 98.24% for 180 min (Table 2). The photocatalytic activity of bimetallic MOFs La-Y-PTC is higher than La-PTC and Y-PTC due to the substitution of yttrium metal against lanthanum in MOFs encourages the transfer of electrons from the metal to metal. It can inhibit the photoexcited electron-hole recombination that leads to the decreasing photocatalytic activity. Guo *et al.* successfully synthesized ZIF-67@Co-MOF-74 with better photocatalytic activity than ZIF-67 and Co-MOF-74 [23]. An illustration of the transfer of metal-metal electrons can be seen in Figure 7.

3.3 Effect of Methylene Blue Concentration

Figure 8(a) shows the degradation efficiency of methylene blue at 10, 15, 20, 25 and 30 ppm are 98.24; 71.02; 63.96; 42.18 and 17.42%, respectively. At concentrations of 10, 15 and 20 ppm, the degradation efficiency increases every 30 min. However, at 25 and 30 ppm, its degradation efficiency tends to go up and down. It showed the removal of MB was carried out only by adsorption mechanism.

The dyes' adsorption on the photocatalyst's surface influenced the photocatalytic degradation rate. In the photocatalytic degradation process, only dyes that adsorbed on the photocatalyst surface are degraded. In general, the greater the initial concentration decreases its degradation efficiency. Since the number of photons (hv) that can penetrate the surface of the photocatalyst is getting less due to the obstruction of substance molecules that cover the surface of the photocatalyst, and then the hydroxyl radicals (•OH) that are an essential factor in the degradation of the dye are challenging to form [25]. In addition, the decreasing degradation efficiency is due to the photocatalyst already in the saturated phase due to the high concentration of dyes. Already saturated

Table 2. Dyes degradation comparison between bimetallic MOF La-Y-PTC, La-PTC and Ya-PTC.

MOF	Initial dyes concentration (ppm)	MOF dosage (% b/v)	pH and Light source	Time (min)	Degradation efficiency (%)	Ref.
La-PTC	MB 10	0.06	pH = 7, mercury lamp	240	No photocatalytic	[14]
	MO 10	0.06			64.74	
Y-PTC	MB 10	0.06	pH = 7, mercury lamp	240	87.55	[15]
	MO 10	0.06			50.89	
La-Y-PTC	MB 10	0.05	pH = 7	180	98.24	This work
	MB 20	0.05	pH = 2, mercury lamp		69.57	
	MO 10	0.05			93.63	

photocatalysts decrease photon efficiency and cause photocatalyst deactivation [26]. Krishnan *et al.* explain that increasing dyes concentration from 20 ppm to 60 ppm enhances degradation efficiency [27]. Still, the degradation efficiency has decreased to a concentration of 100 ppm. Samuel *et al.* also reported that the increasing concentration of 4-nitrophenols from 5 ppm to 10 ppm gives the enhancing degradation efficiency of Zn(BDC)(DMF), but when the concentration is 40 ppm, the efficiency decreases significantly [28].

3.4 Effect of MOFs La-Y-PTC Dosage

Figure 8(b) shows photocatalyst dosage of 5, 15, 25, 35 and 45 mg having successive degradation efficiency of 12.75; 20.24; 63.96; 54.00 and 47.18%. The optimum La-Y-PTC dosage is 25 mg. The La-Y-PTC dosages at 5 and 15 mg have a fluctuating trendline. Due to the small number of catalysts, their photocatalytic activity is disturbed. Whilst at 35 and 45 mg, there is a fluctuating trendline resulting from too abundant photocatalyst particles that causes turbidity in the solution. Kumar & Pandey explained that the active site where the reaction occurs was increased by increasing the photocatalyst dosage [25]. It contributed to the higher radicals (•OH) number formed. However, too many photocatalysts affect the turbidity of the solution. A cloudy solution causes the rays to be challenging to reach the active site of the photocatalyst so that electron excitation and radical formation (•OH) become inhibited, resulting in decreased degradation [25].

3.5 The pHpzc point of la-Y-PTC and Effect of pH

Figure 8(c) shows a methylene blue degradation efficiency of 69.57; 52.06; 63.96; 65.29 and 73.83% for pH 2, 5, 7, 9 and 11. The alkaline condition at pH 9 and 11 (Figure 8(c)) show there is a fluctuating trendline of MB degradation efficiency. It confirmed that the MB decolorization was more affected by adsorption ability than photocatalytic activity of La-Y-PTC. It is due to the bimetallic MOF La-Y-PTC consisting of lanthanum and yttrium metals with carboxylic ion linkers, a group of hard acids and hard bases that unstable in alkaline condition. Then, MOF was decomposed by OH^- ions, and lost its photocatalytic activity.

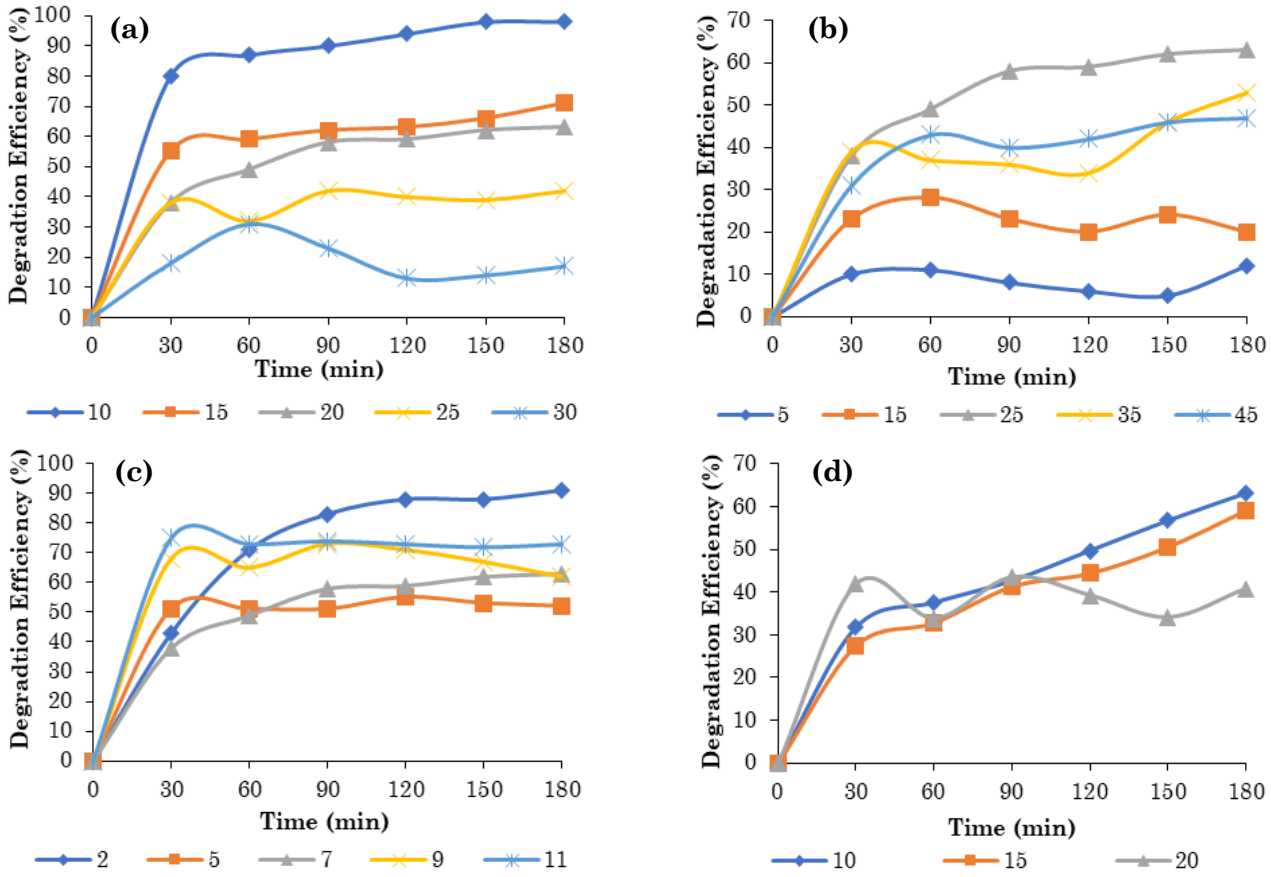

Figure 8. Methylene blue degradation efficiency at various initial concentrations of methylene blue (a); La-Y-PTC dosage (b); initial pH solution (c); and concentration of methyl orange (d).

The decolorization percentage of MB at alkaline condition (pH = 9 and pH = 11) is higher than at acidic and neutral condition. The initial pH affects the La-Y-PTC surface charge, and generate the change of its adsorption ability. The increasing of MB adsorption was influenced by the increasing of electrostatic force attraction. The pHpzc of La-Y-PTC was found to be 6.90 (Figure 9). It confirmed that at higher pH (pH>pHpzc), namely pH = 9 and pH = 11, the MOF La-Y-PTC surface become negatively charged. Therefore, the cationic dye (MB) adsorption will be more favorable. At pH = 11, decolorization of MB is higher than pH = 9. It is due to the high pH increase the number of OH^- ions on the La-Y-PTC surface, and encourage the MB adsorption via electrostatic interaction [29].

In contrast, pH = 2 has a trendline that continues to rise. Acidic conditions cause the photocatalyst surface to be more positively charged. So that, the MB adsorption by La-Y-PTC is unfavorable because of the electrostatic repulsion between similar charge La-YPTC surface and MB [25]. It explained that the degradation efficiency of MB by La-Y-PTC was influenced by photocatalytic mechanism than adsorption mechanism. At pH = 2, hydrogen (H^+) ion will capture the electrons towards the La-Y-PTC surface, inhibit the electron-hole pairs recombination process, so that the photocatalytic activity was increased [30]. Zebardast *et al.* succeeded in synthesizing Co/Zn-MOF-5 and Ni/Zn-MOF-5, which degrade methylene blue 12 ppm at a pH of 2-4 with a degradation efficiency of 80-90% [31].

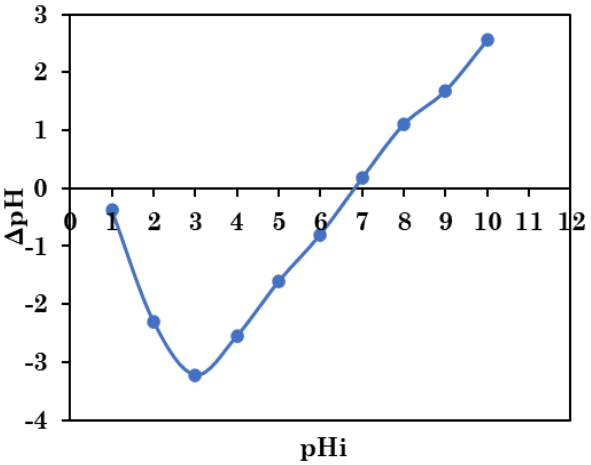

Figure 9. The point of zero charge of MOF La-Y-PTC.

3.6 Methyl Orange Degradation by Bimetallic MOFs La-Y-PTC

Figure 8(d) shows that at pH 2, the degradation efficiency of methyl orange 20 ppm has a fluctuating value with a degradation efficiency of 40.76% for 180 min. In contrast, the concentrations of 10 ppm performed good photocatalytic degradation with a degradation efficiency of 93.63%, and 15 ppm reached 59.11%. The concentration of methyl orange affects the magnitude of their degradation efficiency. Samuel *et al.* proved that there is an increase in the concentration of 4-nitrophenols from 5 ppm to 10 ppm, which is the result of a degradation efficiency Zn(BDC)(DMF) that is increasing [28]. Still, if the concentration is increased to 40 ppm, the degradation decreases significantly.

Besides that, the pH of the solution also affects photocatalytic reactions. It is because pH affects the active sites on the photocatalyst's surface. Methyl orange, an anionic dye, has excellent photocatalytic degradation in acidic conditions (pH<7) due to an electrostatic bond between the methyl orange and the photocatalyst surface charge. Conversely, in alkaline conditions, the photocatalyst surface is negatively charged, so there is a repulsive force between the methyl orange and the photocatalyst surface, reducing its degradation efficiency [32].

3.7 Methylene Blue and Methyl Orange Degradation by Bimetallic MOF La-Y-PTC

Figure 10 shows the bimetallic MOF of La-Y-PTC capable of degrading both types of dyes, namely methylene blue and methyl orange, with degradation capacities of 27.83 mg/g and 18.73 mg/g, respectively. The degradation efficiency of methylene blue is greater than that of methyl orange. The reaction condition occurs in an acidic (pH = 2). Under acidic conditions, hydrogen ions capture electrons forming so that the recombination rate of electron pairs is excited and the electron-hole becomes inhibited, increasing their photocatalytic activity [30].

pH influences methyl orange degradation by affecting the active site on the photocatalyst surface charge. In acidic conditions, hydrogen ions (H^+) made the photocatalyst surface more positively charged. Therefore, methyl orange's degradation efficiency increases at the lower pH of the solution. Conversely, methyl orange is an anionic dye that becomes well degradable at acidic pH due to the increase in photocatalyst adsorption ability against methyl orange by the electrostatic interaction between nega-

tively charged methyl orange and positively charged photocatalyst surfaces [32].

The adsorption of their photocatalysts influences the photo degradability of dyes. It is because degraded dye molecules are molecules that are absorbed on the surface of the photocatalyst. Under acidic conditions, methylene blue is adsorbed on the surface of La-Y-PTC, weaker than methyl orange. It is because methylene blue is adsorbed only through hydrogen and π bonds. In contrast, methyl-orange is adsorbed through hydrogen interactions, π, and electrostatic bonds between the negative charges in methyl orange and photocatalysts that tend to be more positively charged. The bond strength between methylene blue and photocatalyst is weaker, so it is easier to degrade than methyl orange. So, methylene blue's degradation is more remarkable than methyl orange. Photocatalytic activity tests evidence it on a mixture of methyl orange and methylene blue solution. The test results showed that the photodegradation rate of methylene blue was faster than methyl orange (Figure 10). MOFs La-Y-PTC can degrade methylene blue with a degradation efficiency of 90.05% within 30 min, while methylene orange degrades by 92.36% within 120 min.

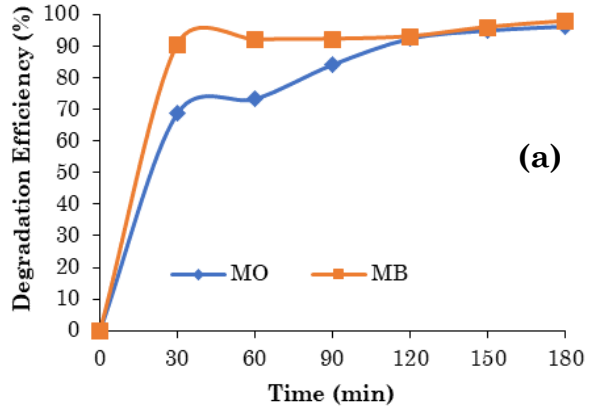

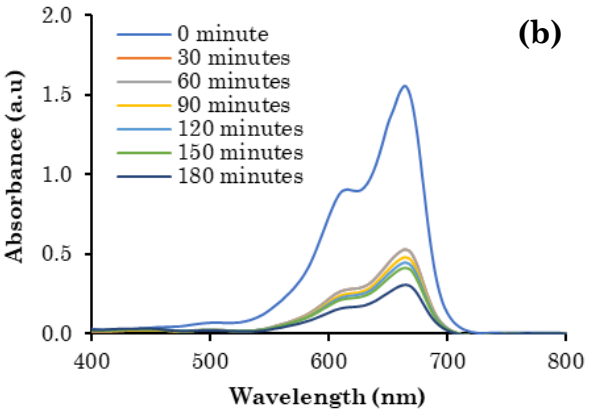

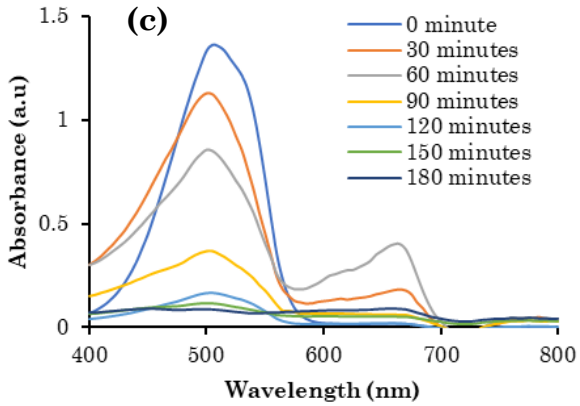

Figure 10. Methylene blue (MB) and methyl orange (MO) degradation efficiency (a); UV-Vis spectrum of MB (b); and MO (c) after and before reaction.

Figure 10 also exhibits that the MB and MO were degraded by MOF La-Y-PTC to obtain carbon dioxide and water as the final product. It can be seen from the UV-Vis spectrum of MB and MO (Figure 10(b) and (c)) that show no new peak or the maximum wavelength was formed. The MB and MO degradation were affected by the free radical species such as hydroxyl and superoxide that were obtained by the reaction between photoexcited electron-hole pairs and H_2O and O_2 that were adsorbed on the La-Y-PTC surface [33]. The mechanism of hydroxyl and superoxide radical can be seen in Equations (2)-(4).

$$\text{MOFs} + h\nu \rightarrow \text{MOFs}\ (e^-_{cb} + h^+_{cb}) \quad (2)$$

$$h^+_{vb} + H_2O \rightarrow \cdot OH + H^+ \quad (3)$$

$$e^-_{cb} + O_2 \rightarrow \cdot O_2^- \quad (4)$$

3.8 Dominant Species in Photocatalytic Activity of Methylene Blue and Methyl Orange

Adding H_2O_2 0.1 M increased the degradation efficiency from 69.57% to 84.28% for methylene blue and methyl orange from 40.76% to 96.88% (Figure 11). Adding H_2O_2 increases free radical species (•OH) formation, which contributes significantly to photocatalytic degradation reactions. H_2O_2 added to the system captures photoexcited electrons to prevent recombination between photoexcited electron and electron-hole pairs [34]. In addition, H_2O_2 also reacts with photoexcited electrons producing radicals (•OH) and hydroxide ions (OH^-) [34].

Furthermore, the electron holes in the valence band in the La-Y-PTC will be stabilized through bonds with hydroxide ions or other species, such as water, producing hydroxyl radicals (•OH). On the other hand, H_2O_2 was also decomposed by light-producing hydroxyl radicals (•OH). The increasing number of hydroxyl

radicals increases the efficiency of methylene blue degradation [34]. The mechanism can be written by Equations (5)-(9).

$$MOFs + h\upsilon \rightarrow MOFs\ (e^-_{cb} + h^+_{cb}) \quad (5)$$
$$e^-_{cb} + H_2O_2 \rightarrow \cdot OH + OH \quad (6)$$
$$e^-_{cb} + O_2 \rightarrow \cdot O_2^- \quad (7)$$
$$h^+_{vb} + OH^- \rightarrow \cdot OH \quad (8)$$
$$h^+_{vb} + H_2O_2 \rightarrow 2 \cdot OH \quad (9)$$

Meanwhile, for the addition of methanol, there was a decrease in the degradation efficiency of methylene blue to 38.42%. Figure 11 also shows the fluctuating value of methylene blue degradation efficiency. It suggests that adding methanol causes the MOFs La-Y-PTC to lose its photocatalytic activity against methylene blue. In contrast to methylene blue, the degradation efficiency of methyl orange has increased from 40.76% to 72.61%. However, adding methanol results in a lower methyl orange degradation efficiency than adding hydrogen peroxide. Methanol causes electron holes (h^+) to oxidize to hydroxyalkyl radicals ($\cdot CH_2OH$), which oxidize further to formaldehyde (CH_2O) [34]. Thus, in this case, there is no formation of hydroxyl radicals ($\cdot OH$) that play an essential role in the photodegradation process of methylene blue.

On the other hand, the photoexcited electrons react with oxygen adsorbed on the surface of MOFs to form superoxide radicals ($\cdot O_2^-$). The radicals also react with dyes to form degradation products [34]. These results indicate that the dominant species that play a role in the photocatalytic process of degradation of methylene blue and methyl orange by MOFs La-Y-PTC are hydroxyl radicals ($\cdot OH$) and electron holes (h^+). It also proves the results of previous tests where MOFs La-Y-PTC was able to degrade the two dyes because hydroxyl radical species reduced the concentration of dyestuffs non-selectively [35,36]. The degradation mechanism in the presence of methanol addition is shown in Equations (10)-(13).

$$MOFs + h\upsilon \rightarrow MOFs\ (e^-_{cb} + h^+_{vb}) \quad (10)$$
$$h^+_{vb} + CH_3OH \rightarrow \cdot CH_2OH \rightarrow CH_2O \quad (11)$$
$$e^-_{cb} + O_2 \rightarrow \cdot O_2^- \quad (12)$$
$$MB + \cdot O_2 \rightarrow H_2O + CO_2 \quad (13)$$

In addition, the role of hydroxyl radicals in the degradation of methylene blue and methyl orange is also evidenced by testing photocatalytic activity with a mixture of tertiary butanol (tert-BuOH) and H_2O_2. Figure 11 showed a decrease in degradation efficiency to 63.16% and 95.10% for methylene blue and methyl orange, respectively. Tert-BuOH captures hydroxyl radicals, reduces the number of hydroxyl radicals that play a role in the degradation process, and decreases degradation efficiency.

4. Conclusion

This study has successfully synthesized the bimetallic MOF La-Y-PTC by solvothermal method. The synthesized bimetallic MOF La-Y-PTC showed higher degradation efficiency to methylene blue and methyl orange than monometallic MOFs La-PTC and Y-PTC. The photocatalytic degradation of methylene blue and methyl orange by bimetallic MOFs La-Y-PTC occurs through forming of hydroxyl free radical species. This study shows that the combining lanthanum and yttrium metal ion in enhances their photocatalytic activity for both MB and MO degradation.

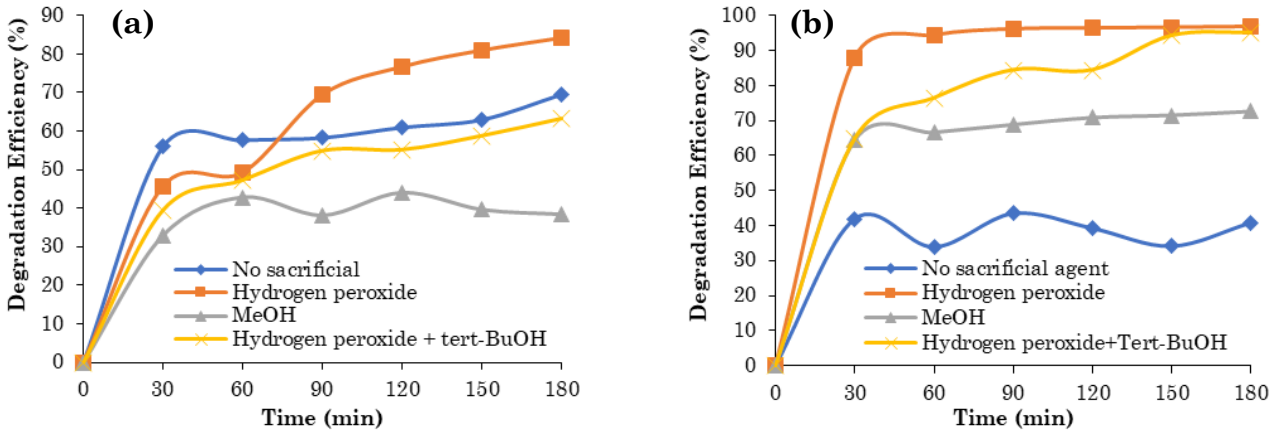

Figure 11. Degradation efficiency of (a) methylene blue and (b) methyl orange in the presence of the addition of hydrogen peroxide (H_2O_2), methanol (MeOH) and tertiary butanol (tert-BuOH).

Acknowledgment

The authors wish to thank UIN Syarif Hidayatullah Jakarta for financial support under the contract number B-205/LP2M-PUSLITPEN/TL.03/06/2021.

CRediT Author Statement

A. Adawiah was responsible for conceptualization, validation, resources, data curation, writing, review, and editing; M. S. Gunawan was responsible for formal analysis, investigation, data collection, and draft preparation. I. Aziz was in command of writing, reviewing, and editing. W. Octavia discussed research, resources, and draft preparation. All authors read the manuscript and promptly approved it in the published version.

References

[1] Priya, A.K., Pachaiappan, R., Kumar, P.S., Jalil and Vo, D.V.N., Rejendran, S. (2021). The War using microbes: a sustainable approach for wastewater management. *Environmental Pollution*. 275, 116598. DOI:10.1016/j.envpol.2021.116598.

[2] Saeed, M., Usman, M., Haq, A.ul. (2018). Catalytic degradation of organic dyes in aqueous mediom photochemistry and photophysics. *Fundamentals to Application*. 198-208. DOI: 10.5772/intechopen.75008.

[3] Tan, K.A., Morad, N., Ooi, J.Q. (2016). Phytoremediation of methylene blue and methyl orange using Eichhornia crassipes. *International Journal of Environmental Science and Development*. 7(10), 724-728. DOI: 10.18178/ijesd.2016.7.10.869.

[4] Sun, L., Hu, D., Zhang, Z., Deng, X. (2019). Oxidative degradation of methylene blue via pds-based advanced oxidation process using natural pyrite. *International Journal of Environmental Research and Public Health*. 16(23), 4773. DOI: 10.3390/ijerph16234773.

[5] Ahmad, A., Mohd-Setapar, S.H., Chuong, C.S., Khatoon, A., Wani, W.A., Kumar, Rafatullah, M. (2015). Recent advances in new generation dye removal technologies: novel search for approaches to reprocess wastewater. *RSC Advances*. 5(39), 30801-30818. DOI: 10.1039/C4RA16959J.

[6] Maslukah, L., Yudiati, E. (2017). Model adsorpsi logam berat pb, cu dan zn sistem air-sedimen muara sungai banjir kanal barat Semarang. *Maspari Journal*. 9(2), 149–158. DOI: 10.56064/maspari.v9i2.4484.

[7] Nitsae, M., Solle, H.R.L., Martinus, S.M., Emola, I.J. (2021). Studi adsorpsi metilen biru menggunakan arang aktif tempurung lontar (*Borassus flabellifer* L.) Asal Nusa Tenggara Timur. *Jurnal Kimia Riset*, 6(1), 46–57. DOI: 10.20473/jkr.v6i1.24525.

[8] Permatasari, T.J., Apriliani, E., Matematika, J., Matematika, F., Alam, P., Ii, K., Di, I.I.I. (2013). Optimasi penggunaan koagulan dalam proses penjernihan air. *Jurnal Sains dan Seni Pomits*, 2(1), 6. DOI 10.12962/j23373520.v2i1.3054.

[9] Suryandari, A.S., Mustain, A., Pratama, D.W., Maula, I. (2019). Studi aktivitas reaksi fotokatalisis berbasis katalis TiO_2-karbon aktif terhadap mutu air limbah power plant. *Jurnal Teknik Kimia dan Lingkungan*, 3(2), 95–101. DOI: 10.33795/jtkl.v3i2.124.

[10] Li, H.P., Dou, Z., Chen, S.Q., Hu, M., Li, S., Sun, H.M., Jiang, Y., Zhai, Q.G. (2019). Design of a multifunctional indium-organic framework: fluorescent sensing of nitro compounds, physical adsorption, and photocatalytic degradation of organic dyes. *Inorganic Chemistry*, 58(16), 11220-11230. DOI: 10.1021/acs.inorgchem.9b01862.

[11] Zulys, A., Adawiah, A., Gunlazuardi, J., Yudhi, M.D.L. (2021). Light-harvesting metal-organic frameworks (MOFs) La-PTC for photocatalytic dyes degradation. *Bulletin of Chemical Reaction Engineering & Catalysis*, 16(1), 170-178. DOI: 10.9767/bcrec.16.1.10309.170-178.

[12] Adawiah, A., Yudhi, M.D.L., Zulys, A. (2021). Photocatalytic degradation of methylene blue and methyl orange by Y-PTC metal-organic framework. *Jurnal Kimia Valensi*, 7(2), 129-141. DOI: 10.15408/jkv.v7i2.22267.

[13] Arora, C., Soni, S., Sahu, S., Mittal, J., Kumar, P., Bajpai, P.K. (2019). Iron based metal organic framework for efficient removal of methylene blue dye from industrial waste. *Journal of Molecular Liquids*, 284, 343-352. DOI: 10.1016/j.molliq.2019.04.012.

[14] Herrera, L.A.Á., Reyes, P.K.C., Flores, A.M.H., Martínez, L.T., Villanueva, J.M.R. (2020). BDC-Zn MOF sensitization by mo/mb adsorption for photocatalytic hydrogen evolution under solar light. *Materials Science in Semiconductor Processing*, 109(1), 1-7. DOI: 10.1016/j.mssp.2020.104950.

[15] Tiwari, A., Sagara, P.S., Varma, V., Randhawa, J.K. (2019). Bimetallic metal organic frameworks as magnetically separable heterogeneous catalysts and photocatalytic dye degradation. *ChemPlusChem*, 84(1), 136-141. DOI: 10.1002/cplu.201800546.

[16] Reddy, M.C., Sivaramakrishna, L., Reddy, A. (2012). The use of an agricultural waste material, Jujuba seeds for the removal of anionic dye (Congo red) from aqueous medium. *Journal of Hazardous Materials*, 203–204, 118–127. DOI: 10.1016/j.jhazmat.2011.11.083.

[17] Prabhu, S.M., Imamura, S., Sasaki, K. (2019). Mono-, di-, and tricarboxylic acid facilitated lanthanum-based organic frameworks: insights into the structural stability and mechanistic approach for superior adsorption of arsenate from water [research-article]. *ACS Sustainable Chemistry and Engineering*, 7(7), 6917-6928. DOI: 10.1021/acssuschemeng.8b06489.

[18] Yang, T., Xiang, Q., Feng, L., Dong, C., Zhang, X., Ning, Z., Lai, X. (2019) Yttrium-based metal-organic frameworks: controllable synthesis, growth mechanism and the phase transformation to Y_2O_3: Eu^{3+} Phosphors. *Journal of Luminescene*, 214(3), 116567. DOI: 10.1016/j.jlumin.2019.116567.

[19] Shadmehr, J., Zeinali, S., Tohidi, M. (2019). Synthesis of a chromium terephthalate metal organic framework and use as nanoporous adsorbent for removal of diazinon organophosphorus insecticide from aqueous media. *Journal of Dispersion Science and Technology*, 40(10), 1423-1440. DOI: 10.1080/01932691.2018.1516149.

[20] Lin, C. K., Zhao, D., Gao, W.Y., Yang, Z., Ye, J., Xu, T., Ge, Q., Ma, S., Liu, D.J. (2012). Tunability of band gaps in metal-organic frameworks. *Inorganic Chemistry*, 51(16), 9039–9044. DOI: 10.1021/ic301189m.

[21] Chen, L., Wang, H. F., Li, C., Xu, Q. (2020). Bimetallic metal-organic frameworks and their derivatives. *Chemical Science*, 11(21), 5369–5403. DOI: 10.1039/D0SC01432J.

[22] Behrsing, T., Deacon, G.B., Junk, P.C. (2014). *The Chemistry of Rare Earth Metals, Compounds, and Corrosion Inhibitors*. in In Rare Earth-Based Corrosion Inhibitors, Australia, Woodhead Publishing Limited. 1-37. DOI: 10.1533/9780857093585.1.

[23] Guo, C., Guo, J., Zhang, Y., Wang, D., Zhang, L., Guo, Y., Ma, W., Wang, J. (2018). Synthesis of core-shell ZIF-67@Co-MOF-74 catalyst with controllable shell thickness and enhanced photocatalytic activity for visible light-driven water oxidation. *CrystEngComm*, 20(47), 7659-7665. DOI: 10.1039/C8CE01266K.

[24] Kumari, A., Kaushal, S., Singh, P.P. (2021). Bimetallic metal organic frameworks heterogeneous catalysts: design, construction, and applications. *Materials Today Energy*, 20, 100667. DOI: 10.1016/j.mtener.2021.100667.

[25] Kumar, A., Pandey, G. (2017). A review on the factors affecting the photocatalytic degradation of hazardous materials. *Material Science & Engineering International Journal*, 1(3), 106–114. DOI: 10.15406/mseij.2017.01.00018.

[26] Chen, X., Mao, S. S. (2007). Titanium dioxide nanomaterials: synthesis, properties, modifications and applications. *Chemical Reviews*, 107(7), 2891–2959. DOI: 10.1021/cr0500535.

[27] Krishnan, J., Arvind Kishore, A., Suresh, A., Madhumeetha, B., Gnana Prakash, D. (2017). Effect of pH, inoculum dose and initial dye concentration on the removal of azo dye mixture under aerobic conditions. *International Biodeterioration and Biodegradation*, 119, 16-27. DOI: 10.1016/j.ibiod.2016.11.024.

[28] Samuel, M.S., Bhattacharya, J., Parthiban, C., Viswanathan, G., Pradeep Singh, N.D. (2018). Ultrasound-assisted synthesis of metal organic framework for the photocatalytic reduction of 4-nitrophenol under direct sunlight. *Ultrasonics Sonochemistry*, 49, 215-221. DOI: 10.1016/j.ultsonch.2018.08.004.

[29] Zein, R., Chaidir, Z., Zilfa, Z., Fauzia, S., Ramadhani, P. (2022). Isotherm and Kinetic Studies on the Adsorption Behavior of Metanil Yellow Dyes onto Modified Shrimp Shell-Polyethylenimine (SS-PEI). *Jurnal Kimia Valensi*, 8(1), 10-22. DOI: 10.15408/jkv.v8i1.22566.

[30] Yin, X.J., Zhu, L.G. (2019). High-efficiency photocatalytic performance and mechanism of silver-based metal–organic framework. *Journal of Materials Research*, 34(6), 991–998. DOI: 10.1557/jmr.2018.507.

[31] Zebardast, M., Shojaei, A.F., Tabatabaeian, K. (2018). Enhanced removal of methylene blue dye by bimetallic nano-sized MOF-5s. *Iranian Journal of Catalyst*, 8(4), 297-309.

[32] Khade, G.V., Gavade, N.L., Suwarnkar, M.B., Dhanavade, M.J., Sonawane, K.D., Garadkar, K. (2017). Enhanced photocatalytic activity of europium doped tio_2 under sunlight for the degradation of methyl orange. *Journal of Materials Science: Material in Electronics*. 28(15), 11002-11011. DOI: 10.1007/s10854-017-6883-9.

[33] Pingmuang, K., Chen, J., Kangwansupamonkon, W., Wallace, G.G., Phanichphant, S., Nattestad, A. (2017). Composite photocatalysts containing $bivo_4$ for degradation of cationic dyes. *Scientific Reports*, 7, 1-11. DOI: 10.1038/s41598-017-09514-5.

[34] Samsudin, M.F.R., Lim, T.S., Sufian, S., Bashiri, R., Muti, M.N., Mahirah, R.R. (2018). Exploring the role of electron-hole scavengers on optimizing the photocatalytic performance of $BiVO_4$. *Materials Today: Proceedings*, 5(10), 21703-21709. DOI: 10.1016/j.matpr.2018.07.022.

[35] Yahya, N., Aziz, F., Jamaludin, N.A., Mutalib, M.A., Ismail, A.F., Salleh, W.N.W., Jaafar, J., Yusof, N., Ludin, N.A. (2018). A review of integrated photocatalyst adsorbents for wastewater treatment. *Environmental Chemical Engineering*, 06(051), 1–55. DOI: 10.1016/j.jece.2018.06.

[36] Shayegan, Z., Lee, C.S., Haghighat, F. (2018). TiO_2 photocatalyst for removal of volatile organic compounds in gas phase – a review. *Chemical Engineering Journal*, 334, 2408-2439. DOI: 10.1016/j.cej.2017.09.153.